Evolution of reproduction driven by ecology at the onset of multicellularity

Alexandre Porcher Fernandes[1,2,✉], **Renske M. A. Vroomans**[1,2], **and Enrico Sandro Colizzi**[2,3,✉]

[1]The Sainsbury Laboratory, University of Cambridge, 47 Bateman Street, Cambridge CB2 1LR, UK

[2]Department of Genetics, Downing Site, University of Cambridge, Cambridge CB2 3EJ, UK

[3]Centre INRIA de Lyon, Villeurbanne, Auvergne-Rhône-Alpes, France

Correspondence: *Alexandre.PorcherFernandes@slcu.cam.ac.uk; enrico-sandro.colizzi@inria.fr*

During the transition to multicellularity, nascent multicellular organisms evolved reproductive strategies that relied on coordinating behaviour across cells in the group. Cell-cell interactions that once occurred between independent single-celled organisms in an ecological context were integrated into the developmental programs of emerging multicellular forms. To study this transition, we developed a spatially structured evolutionary model in which cells can migrate, divide, and adhere to neighbours — behaviours common to most unicellular eukaryotes. When coupled to a selective pressure driven by food scarcity, the model reveals how ecological interactions between single cells can give rise to multicellular reproductive programs. We show that a life cycle alternating cohesive multicellular clusters and dispersive unicellular propagules — the most prevalent reproductive strategy in multicellular life — evolves spontaneously as a dispersal strategy in environments where food is concentrated in patches of intermediate size. More broadly, the spatial distribution of food strongly shaped evolutionary outcomes: environments where food was homogeneously distributed favoured unicellular life cycles, while those where food was heterogeneously distributed favoured multicellular life cycles. Furthermore, we show that ancestral unicellular and multicellular life cycles were co-opted and encapsulated as phases of the reproductive programs of propagule-forming lineages during evolution. Taken together, our results highlight how ecological interactions can be repurposed to organise development during the transition to multicellularity.

Reproduction is the central process that drives biological evolution because it structures how genetic information is propagated across generations. During the transition to multicellularity, novel mechanisms evolved that supported reproduction at the level of groups of cells. While unicellular organisms reproduce through cell division, multicellular reproduction is a collective process that requires coordination of cell division, collective behaviour, and spatial organisation to generate a new individual. Modern multicellular organisms have evolved a diverse array of reproductive strategies, which can be broadly divided into two main categories [1, 2]: (i) unicellular propagation, where the organism reproduces by generating single-celled reproductive units, and (ii) multicellular propagation, where the organism splits into two multicellular parts of equal or unequal size. Unicellular propagation is abundant across the tree of life, including sexual reproduction through gametes and formation of unicellular vegetative propagules or spores [3, 4]. Although not as common as unicellular propagation, multicellular propagation occurs in all major multicellular clades, including bacteria [5, 6], algae [7], fungi [8], plants [9, 10], and animals [11, 12] (see [13, 14] for comprehensive reviews of multicellular life cycles). Additionally, both forms of reproduction have been observed to evolve in wet-lab experiments [15–18].

But what drives the evolution of different reproductive strategies? Computational models have suggested that unicellular propagules reduce genetic conflicts between cells within the multicellular organism [19, 20] or slow down the accumulation of mutations [1]. Conversely, multicellular reproduction can be advantageous in cell clusters with rigid cell connections that limit cell division, enabling cell growth in regions previously constrained by the cluster's geometry [21]. More broadly, the selective advantage of unicellular or multicellular replication may depend on how cell birth and death rates scale with group size [22] and on the effect of cooperation between cells in multicellular groups [23].

The ecological context also plays an important role in shaping the evolution of multicellular reproduction. Many organisms have evolved unicellular propagules, such as spores, pollen, or cysts, that can disperse passively via wind or water and are often more resistant to environmental stress than their multicellular progenitors. This makes them well-suited for survival in harsh environments and an effective means of dispersal. Models suggest that diverse life cycles, including those alternating between unicellular and multicellular stages, can evolve in response to fluctuating environments [24, 25], or arise through self-organisation of multicellular groups that can reproduce autonomously

due to adhesion interactions between cells [26]. The predicted influence of the environment on the evolution of multicellular reproduction is also evident in nature, where seasonal fluctuations in nutrient availability regulate life cycle transitions in many eukaryotes. For example, nutrient scarcity triggers the multicellular phase in the life cycle of the slime mould *Dictyostelium discoideum*, whereas the Holomycota *Fonticula alba* forms collective feeding streams only when bacterial food is available [27].

The ecological and genetic contexts have also played a role in the origin of multicellularity itself. As cells formed tighter associations during the transition to multicellularity, new ecological functions such as predation avoidance [15, 18] or enhanced resource capture [28], selected for traits that increased group sizes, improved the spatial integrity of the cluster, and mediated collective responses to environmental fluctuations [29]. Comparative phylogenetic studies show that these selective demands at the onset of multicellularity were largely met by coopting the pre-existing molecular toolkit [30, 31]: proteins used for adhesion with the substrate or sensing environmental cues were repurposed for intercellular adhesion [32, 33], while cell-cycle and stress regulators became involved in cellular differentiation [34, 35]. However, the contribution of the co-option of these ancestral modules to the evolution of development and reproduction at the onset of multicellularity remains unknown. Promising experimental results show that reproductive propagules can readily evolve after multicellularity, suggesting that they could have evolved via co-option of an ancestral unicellular life cycle [17].

To clarify how ecological pressures influence the spatial organisation of cells during reproduction and how the co-option of ancestral modules enables novel ecological functions, we need a modelling framework that integrates the evolution of gene regulation with ecological interactions between cells and their environment [36, 37]. Existing models, however, typically lack a spatially-explicit environment, abstract away genetic regulation of reproductive behaviour, or restrict the evolution of reproductive strategies to a few, preselected options. To address this issue, we used a bottom-up approach to study the evolution of multicellular reproduction. We developed a model where a population of cells inhabit a structured environment and consume resources to survive and replicate. We model a minimal set of cellular traits, namely intercellular adhesion, chemotaxis, and cell division, that are widespread across the eukaryotic tree of life [4]. With this setup, we investigate how spatially structured ecological interactions among unicellular individuals give rise to reproduction at the onset of multicellularity. We characterise these developmental dynamics and show that they evolve by co-opting pre-existing life-cycles and are stabilised through an eco-evolutionary feedback.

Results

Model setup

To investigate the evolution of reproductive strategies in nascent multicellular organisms, we constructed a hybrid Cellular Potts Model [38] where a population of cells forages for food on two-dimensional space (Fig. 1A). Food is introduced at a constant rate into the environment as circular “patches”, each composed of several food units. The food patches release a chemoattractant, creating a gradient around them that cells can follow to locate and consume resources, which are stored as metabolic reserves. If all the food in a food patch is consumed, it stops generating the chemoattractant signal, allowing cells to re-route to the next source of food. Cells have a constant metabolic rate that depletes their metabolic reserves. When the cell’s reserves are exhausted, it dies and is removed from the lattice. We also include a small uniform probability of death due to other factors, such as predation and metabolic stress, which are not modelled explicitly.

Cellular behaviour is controlled by a Gene Regulatory Network (GRN) composed of sensory, regulatory, and functional genes (Fig. 1B). The sensory genes receive as input the concentration of the chemical signal at the cell’s location and the amount of internal metabolic reserves. These inputs are then processed by a layer of regulatory genes that control the activation of the downstream functional genes. Functional genes dictate cell behaviour. We model a minimal set of cellular behaviours commonly observed in microbial eukaryotes [39–42]: cells can migrate following the chemical signal diffusing from food sources, consume food from the environment, divide, and adhere to their neighbours (Fig. 1C). The cell state — either migrating or dividing — is determined by the output of the first functional gene. We model these two behaviours as mutually exclusive, following the observation that migration and division require conflicting use of the cytoskeleton in many eukaryotes [43–45]. Migrating cells perform chemotaxis by biasing their movement towards the direction of the perceived chemical gradient [46], while dividing cells cannot actively migrate and grow over a fixed period before dividing into two daughter cells. When a cell divides, the parameters of the GRN of one daughter cell can mutate with a small probability, while the other cell inherits the parental parameters. Both daughter cells inherit half of the metabolic reserves of their mother. An additional set of sixteen functional genes encodes adhesion proteins that are expressed on the cell membrane and mediate adhesion between adjacent cells. These proteins are modelled as ligands and receptors, and adhesion strength (γ) between adjacent cells increases with the degree of complementarity between their ligands and receptors (see Methods).

Together, these components create a structured dynamic environment in which individual cells must integrate internal and ecological cues to survive. The mutations to the GRN during cell division introduce genetic variation into the population. This variation, combined with differential survival and reproduction under ecological constraints, drives an evolutionary process without directly specifying its outcome, which is therefore free to emerge spontaneously. In the following sections, we examine how this setup gives rise to diverse life cycles that can coordinate multicellular reproduction.

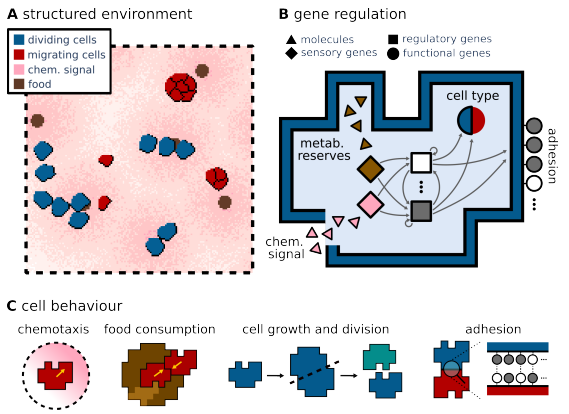

Figure 1. Model setup. **A** Cells live in a structured environment where they forage for resources by following the chemoattractant signal that diffuses from patches of food. Here, a small section of the 2000x2000 lattice is shown. **B** Diagram of a cell's gene regulation. Cell behaviour is controlled by a Boolean GRN that senses the amount of metabolic reserves accumulated in the cell and the strength of the chemoattractant signal. These inputs are processed by a layer of 18 regulatory genes that will determine the cell state (migrating or dividing) and the activation state of the 16 adhesion genes. Active genes are shown in grey, inactive in white. Arrows show the connections between genes in the GRN. **C** We model two cell states: migrating and dividing. Cells can accumulate metabolic reserves by consuming food if they share a lattice site with a food site and adhere to their neighbours when they express complementary combinations of adhesion proteins.

Evolution of diverse life cycles mediated by distribution of resources

Using this setup, we ran 72 simulations each starting with a population of 800 cells. The cells start with a randomised GRN which can evolve throughout the simulation. Simulations ran for 10^8 time steps in one of six environmental conditions (EC 1-6) that differ in the heterogeneity of food distribution. We explore food heterogeneity systematically across ECs, by doubling food patch area and halving creation frequency between successive ECs, while holding total food influx constant (Table S1 and Fig. S1). EC 1 has a relatively even resource distribution, with many small, closely spaced food patches, whereas in EC 6 resources are concentrated into a few large, distant patches. At the end of each simulation, we characterised the dominant evolutionary outcome by extracting the last common ancestor of the population and analysing its behaviour through follow-up simulations without mutations (see Methods, Non-evolutionary simulations).

Three main life cycles evolved across our simulations: a strictly unicellular life cycle, a strictly multicellular life cycle, and a mixed life cycle that is multicellular but regulates the formation of unicellular propagules (Fig. 2A and Videos S1–S4, see Methods, Comparison of life cycles). In all cases, cells have evolved to migrate up the chemoattracting gradient when their metabolic reserves are low, and divide after consuming food from the environment. In the multicellular + unicellular propagules life cycle (Fig. 2A, blue), cells adhere to form multicellular clusters during migration, but stop adhering once they initiate division. These dividing cells are left behind as unicellular propagules, while the multicellular cluster continues migration following a new gradient after local resources are depleted. After dividing, the daughter cells of the unicellular propagule resume migration and re-activate adhesion genes, forming a newborn multicellular cluster that follows the chemoattracting gradient to find new resources, thus completing the life cycle.

Some strictly multicellular lineages also form propagules. In this case, the propagule is multicellular and is formed by dividing cells that downregulate adhesion to migrating cells, while still adhering to each other. We observe a spectrum of multicellular reproductive stratgies: at one end are lineages that genetically encode the formation of propagules by consistently downregulating adhesion between migrating and dividing cells (green in Fig. 2), while at the other end are lineages whose clusters divide rarely, and exclusively by phyisically tearing themselves apart when different parts of the cluster are attracted by separate food patches (yellow in Fig. 2).

Food heterogeneity strongly impacts the evolution of reproductive strategies in the model (Fig. 2B). Strictly unicellular strategies evolve most often when food is homogeneously distributed (EC 1-2), while high-adhesion multicellular strategies usually evolve when food distribution is heterogeneous (EC 5-6). Intermediate environments are characterised by the dominance of unicellular and multicellular propagules (EC 3-4). This diversity of life cycles is reflected in adaptive functional characteristics that aid survival in the environments where each strategy evolved. For example, lineages with a high-adhesion multicellular life cycle have larger cluster sizes when compared to strictly unicellular and propagule-forming lineages, since their cells are concentrated in a few clusters that rarely divide (Fig. 2C). These large multicellular clusters display collective chemotaxis and can migrate faster than small clusters or single cells, since the cells can better integrate spatial information about the patchy chemoattractant signal by pulling and pushing neighbouring cells, thus correcting each other's trajectories towards the source of food [47]. Collective migration, and thus stable multicellularity, becomes more advantageous the longer the distance cells must migrate to reach food, which explains why high-adhesion multicellular life cycles dominate the most heterogeneous

environmental conditions (see Methods, Selective advantages of multicellularity and unicellularity).

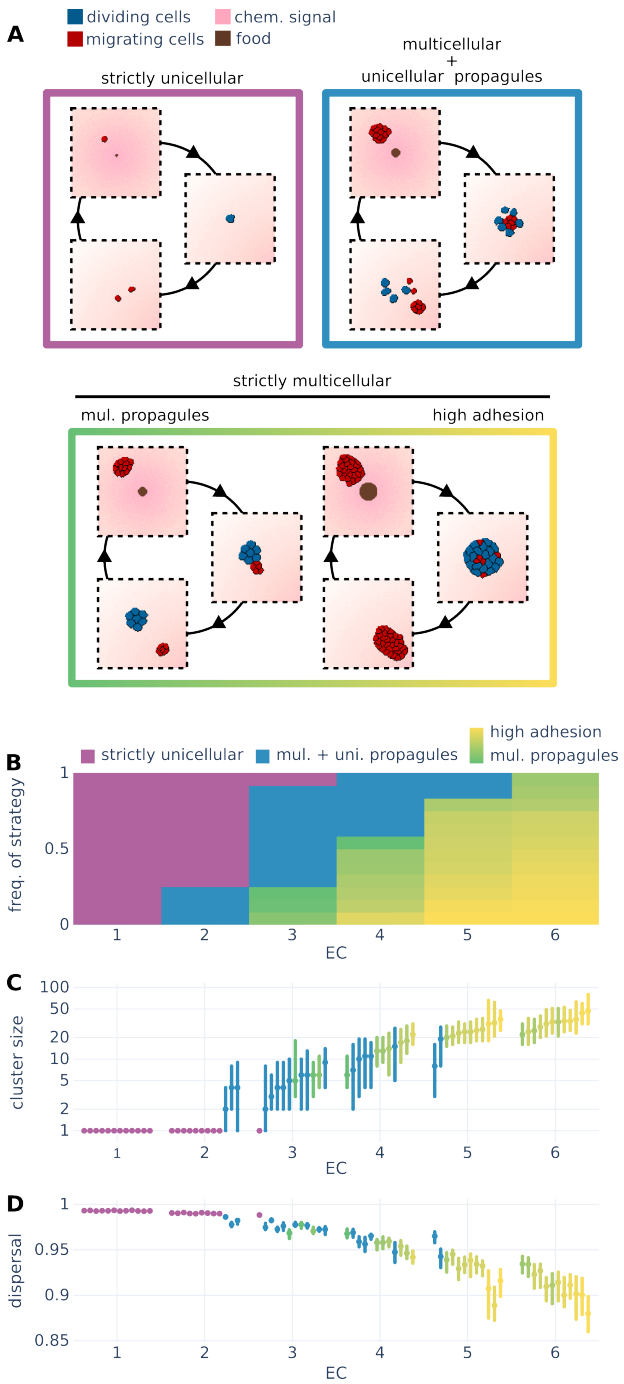

Figure 2. Spatial heterogeneity of resources drives the evolution of complex multicellular life cycles. **A** Three categories of life cycles evolve in our simulations: strictly unicellular, multicellular + unicellular propagules, and strictly multicellular. Strictly multicellular strategies form clusters of dividing cells whose adhesion to the migrating group ranges from loose multicellular propagules that readily detach to highly adhesive groups that rarely split. **B** Distribution of evolved life cycles in different environmental conditions. The colours match the life cycles indicated in A. **C** Cluster sizes and **D** dispersal of all evolved lineages (median and interquartile ranges, see Methods, Measure of dispersal).

Conversely, unicellular lineages disperse better through the environment when compared to multicellular lineages (Fig. 2D). Separating after division helps cells colonise and consume multiple food patches at once, which is especially advantageous when resources are split among many food patches in the most homogeneous environments (see Methods, Selective advantages of multicellularity and unicellularity).

Previous studies suggested that reproduction through single-celled units could have evolved as a mechanism to reduce genetic conflict in populations of clonal multicellular organisms [1, 19]. To determine whether this genetic factor could explain the evolution of single-celled propagules in our model, we analysed the phylogeny of evolved cell populations from the simulations (Fig. S3). We found that the cell clusters of both strictly multicellular and propagule-forming populations are highly heterogeneous due to their aggregative nature, indicating that in this case the reduction of genetic conflicts does not play a role in the evolution of propagules. Instead, the main factor driving the evolution of reproduction via propagules seems to be ecological. In the intermediate environments where unicellular and multicellular propagules evolve, food patches are far apart enough that collective migration is advantageous, while being plentiful enough that dispersal is critical for patch colonisation. As a result, propagule-forming lineages have evolved a multicellular migrating phase that allows them to form clusters to benefit from group migration (Fig. 2C), together with the ability to make unicellular or multicellular propagules for reproduction and dispersal (Fig. 2D).

Development of reproductive strategies: evolved coordination of adhesion and cell state regulation

Because the formation of propagules detaching from migrating clusters emerged spontaneously in our model, we next characterise the regulatory mechanisms that make it possible. We started by quantifying adhesion strength between cells expressing different cell states across our simulations. This shows that propagule-formers coordinate the expression of their cell state and adhesion genes, leading to migrating cells that adhere strongly to other migrating cells but not to dividing cells (Fig. 3A, blue and green). The gene regulatory network achieves this coordination by evolving regulatory genes that co-regulate cell state and the expression profile of adhesion genes, resulting in genetic coupling between the two traits (Fig. S4A). Strictly unicellular and high-adhesion multicellular lineages also often co-regulate cell state and adhesion genes (Fig. S4B), but changes to the expression of adhesion proteins in these cases do not change the adhesion strength between cell states (Fig. 3A, and lineages I, II, IV and V in Fig. S4C).

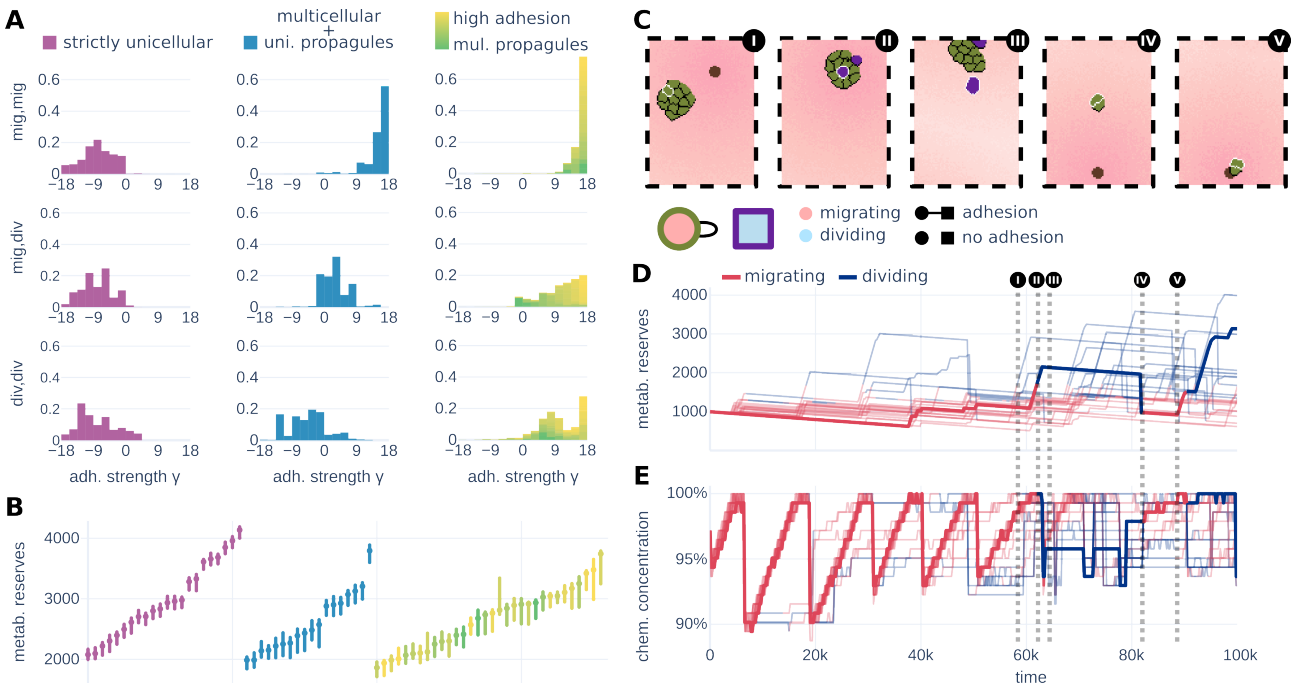

Figure 3. Coordinated expression of cell state and adhesion genes leads to the formation of propagules. **A** Distribution of adhesion strengths (γ) measured across our simulations for cells expressing different pairings of cell states. Propagule-forming life cycles couple the regulation of cell state and adhesion proteins, leading to differential adhesion between pairs of cells according to their cell states (note: $\gamma \lesssim 0$ results in cells detaching from one another). **B** Metabolic reserves are used as a cue for division. We show the interquartile range of threshold values beyond which division is initiated for different lineages. Circles mark the medians. **C** Formation of a unicellular propagule. The colour of the cells indicates which combination of adhesion proteins they express. Below the sequence of images, we show a diagram representing how strongly cells expressing each combination of adhesion proteins adhere to each other. The colour inside the symbol shows whether the combination of adhesion proteins is expressed by cells during migration or division. A line connecting the symbols is drawn if cells expressing the two adhesion profiles adhere. Tracking **D** metabolic reserves, and **E** chemoattractant concentration in a subset of cells over time shows how the GRN uses these values to effect adhesion and behaviour changes. The thicker line represents the trajectory of the cell highlighted in white in C.

We next clarify how the observed adhesion dynamics are regulated by the inputs received by the GRN. In all lineages, cells initiate division when their metabolic reserves exceed a specific value. Because this threshold is genetically encoded (Fig. S4C), the timing of initiation of cell division varies greatly among lineages, but is very consistent within the cells belonging to each lineage (Fig. 3B). In Fig. 3C, we track a cell within a migrating cluster to show how food consumption activates the coordinated regulation of cell division and adhesion, leading to its transition into a propagule. The tracked cell (white border) initially adheres to its migrating cluster using one adhesion profile (step I, green). After feeding, the cell initiates division and expresses a non-adhering combination of adhesion proteins (II, purple), causing it to sort out from the cluster due to differential adhesion [48] and to detach as a propagule (III). After division, the two daughter cells revert to the original adhesion profile and migrate as a new two-celled cluster (IV) that colonises a new food patch (V).

Widespread co-option drives the evolution of propagules

To investigate the evolutionary steps that lead to propagule formation, we extracted strictly unicellular populations from EC 1 and high-adhesion multicellular populations from EC 6 and let them evolve for an additional 10^8 time steps in EC 3, which selects for propagule formation according to our previous evolutionary experiments (Fig. 2). This allowed us to analyse the evolution of life cycles under controlled starting genetic landscapes, where all cells are initially unicellular or multicellular. We observed an increase in the adhesion strength between migrating cells ($\widetilde{\gamma}_{\text{mig,mig}}$) in lineages that were initially strictly unicellular (Fig. 4A, lineage 1), reflecting the establishment of a multicellular migrating phase. Since the adhesion strength between dividing cells and all other cells ($\widetilde{\gamma}_{\text{div}}$) remains low, the lineage is now able to form propagules. Conversely, lineages that were initially high-adhesion multicellular evolve lower $\widetilde{\gamma}_{\text{div}}$ while maintaining high $\widetilde{\gamma}_{\text{mig,mig}}$, indicating that they too have evolved propagule formation (Fig. 4A, lineage 2).

Following individual lineages, we see that propagule formation evolves via co-option of the lineage's ancestral life cycle. Cells in lineage 1 (Fig. 4B) are transferred from EC 1 to EC 3 and initially display a strictly unicellular life cycle (I), with cells expressing a single adhesion profile. The first step towards forming propagules consists of evolving genetic coupling between cell state and adhesion proteins (II): the ancestral adhesion profile (green circle) is now expressed only during migration, while a new profile (purple square) is expressed during division. This change has no immediate functional effect, since the new adhesion profile does not result in cell adhesion. Nevertheless, it represents a pre-adaptation for the subsequent evolution of propagule formation. The critical step (III) to enable the formation of propagules is the evolution of adhesion proteins that cause migrating cells to adhere to each other (dark red triangle), while the expression of the ancestral (green circle) adhesion proteins becomes associated with the dividing cell state. Because there is no adhesion between cells expressing these two adhesion profiles, dividing cells can separate from migrating clusters to form propagules. Once evolved, propagule formation takes over the unicellular population and fixes rapidly (Fig. 4C), highlighting its selective advantage in EC 3. In lineage 2, propagules also evolve via co-option, this time of an ancestral multicellular life cycle. The ancestral combination of adhesion proteins (dark blue dia) is co-opted for the regulation of a migrating phase, followed by the evolution of novel combinations of adhesion proteins (pink triangle and yellow pentagon) that enable propagule formation (4B). The evolution of this trait in lineage 2 also leads to a fast selective sweep in the population (Fig. 4C).

Strictly multicellular lineages seem to have evolved propagule formation more easily than strictly unicellular lineages when transferred to EC 3, evidenced by the fact that 11/12 multicellular lineages evolved a lower $\widetilde{\gamma}_{\text{div}}$, while only 7/12 strictly unicellular lineages evolved a positive $\widetilde{\gamma}_{\text{mig,mig}}$ in the same period of time (Fig. 4D and E). Presumably, this disparity in the number of lineages that evolve propagules is due to the difference in mutation availability between the two cases. Starting from a non-adhering state, most regulatory mutations do not lead to changes in adhesion, creating a large neutral plateau in phenotype space. Thus, strictly unicellular lineages may experience a long series of neutral mutations before reaching a combination that produces adhesion, at which point mutations affecting adhesion proteins become selective. Altogether, this suggests that the initial evolution of adhesion reshapes the accessible evolutionary pathways, facilitating the evolution of subsequent multicellular traits such as propagule formation.

Eco-evolutionary protection of multicellularity

To better understand how environment colonisation and competition could shape ecological dynamics at the onset of multicellularity, we ran a series of experiments where lineages with different life cycles invade ECs 1,3 and 6 and compete with host lineages that evolved in these environments. (Fig. 5A). In most instances, the host lineages — which evolved in the environment where competition is taking place — outcompeted the invading lineages. However, invading lineages with a multicellular + unicellular propagule life cycle outcompeted host lineages in EC 1 in all replicas of the experiment. This prompted us to investigate whether multicellularity could represent a viable strategy in EC 1, despite not evolving there (Fig. 2).

After transferring strictly multicellular and multicellular + unicellular propagule lineages to EC 1 and letting these lineages evolve for 10^8 time steps, we observed that multicellularity persisted in the majority of the simulations

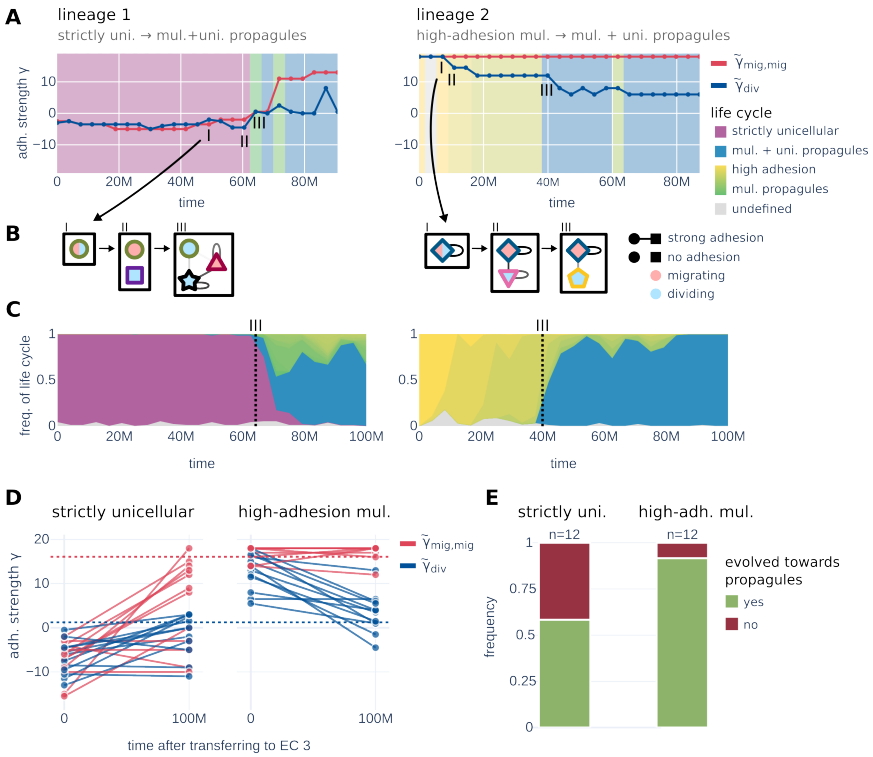

Figure 4. Propagule formation evolves through the co-option of unicellular or multicellular life cycles. **A** Evolution of adhesion properties of a strictly unicellular lineage taken from EC 1 (lineage 1) and a strictly multicellular lineage taken from EC 6 (lineage 2) after their cells are transferred to an environment selecting for propagule formation (EC 3) for 10^8 time steps. The median adhesion strength between migrating cells $\widetilde{\gamma}_{\text{mig,mig}}$ and between dividing cells and all other cells $\widetilde{\gamma}_{\text{div}}$ is shown in red and blue, respectively, with the background colour indicating the life cycle expressed by the lineage at that time (see Methods, Comparison of life cycles). **B** Evolution of regulation of adhesion proteins. Each unique combination of adhesion genes expressed by a lineage is represented by a unique colour and symbol. The inner colour of the symbols indicates whether that combination of adhesion genes is expressed during division or migration. A line connecting the symbols is drawn if cells expressing the two adhesion profiles adhere. **C** Distribution of life cycles among 100 cells taken from the simulations where lineages 1 and 2 originated. Time step III marks the first time propagule formation evolved in lineages 1 and 2. **D** Evolution of $\widetilde{\gamma}_{\text{mig,mig}}$ and $\widetilde{\gamma}_{\text{div}}$ of strictly unicellular lineages (left) and high-adhesion multicellular lineages (right) after they were transferred to EC 3. Dotted lines indicate the average value for the trait in populations endogenous to EC 3. **E** 7 out of the 12 lineages that started with a strictly unicellular life cycle (left) and 11 out of the 12 lineages that started with a high-adhesion life cycle (right) evolved towards making propagules (respectively by increasing their $\widetilde{\gamma}_{\text{mig,mig}}$ and decreasing their $\widetilde{\gamma}_{\text{div}}$, see subfigure D) after being transferred to EC 3.

(35/49, Fig. 5B), with all lineages either preserving or evolving a propagule-forming life cycle (Fig. S6A). Moreover, multicellularity was better protected in lineages that had originally evolved in environments similar to EC 1, as evidenced by the large number of lineages from ECs 5 and 6 that lost multicellularity after the transference. This suggests that protection of multicellularity may be contingent on certain phenotypic or genetic factors. For example, reaching the basin of attraction of the multicellular life cycles that perform well in EC 1 may be easier when starting from specific phenotypes (such as already being able to form propagules) or genetic backgrounds.

In the symmetric experiment, where we transfer strictly unicellular and multicellular + unicellular propagule lineages to EC 6, the inverse pattern can be observed, with a unicellular phase being preserved more often in the ECs that are most different from EC 6 (ECs 1 and 2 in Fig. S6B and C), rather than similar. After being transfered to EC 6, the lineages that preserved a unicellular phase displayed poor fitness. This is also unlike the previous experiment, where the lineages that preserved a multicellular phase performed well in their new environment (compare Fig. S6D and E). Altogether, this suggests that lineages preserving a unicellular phase did not adapt well to EC 6, most likely because they struggled to navigate the phenotype space due to low mutational availability (similarly to the case shown in Fig. 4D and E).

Discussion

In this study, we used a bottom-up approach to investigate the evolution of reproduction in early multicellular species. We find that both unicellular and multicellular modes of reproduction could evolve in our simulations, depending on the heterogeneity of food in the environment. In intermediate environments, cell lineages evolved complex life cycles with a propagule stage, despite the fact that these structures were not specified in the model. These lineages regulate propagule formation by coupling their cell state to specific expression profiles of adhesion proteins. This transient propagulation stage allows for greater dispersal of some daughter cells, while the remaining cells in the multicellular cluster still benefit from collective chemotaxis. We show that these lineages co-opt ancestral strictly unicellular or strictly multicellular life cycles, which are encapsulated as a phase in the developmental cycle of the propagule-forming strategy. Taken together, our results suggest that the emergence of a single- or few-cell stage in a multicellular life cycle is a predictable side-effect of the evolutionary transition to multicellularity.

Comparative genomic and phylogenetic studies have shown that the evolution of multicellular traits involved the co-option of proteins that originally served different functions in their unicellular ancestors [30, 44, 49]. For example, many proteins involved in intercellular adhesion in animals are also found in related unicellular groups, where they perform functions like sensing environmental cues [32] and adhering to the substrate [33]. Similarly, regulatory genes, which are enriched in multicellular species, have evolved from stress regulators [34, 35].

Understanding how reproduction might evolve through such cooption requires models that both include sufficient genetic and regulatory complexity as well as an environment that generates emergent selection pressures for multicellularity [47]. Previously, we showed that emerging multicellular groups act as a new environment in which cells adapt by 'selfishly' maximizing their reproductive success [50]. Here, we expand the regulatory capacity of cells to control both cell state and adhesion protein expression, and we expand the ecological aspect of the model to allow cells to consume food at a higher or lower rate, which allows the cell population to shape its environment during the course of evolution. With this model, we find that co-option can indeed play a central role in the evolution of complex reproduction: both unicellular and multicellular life cycles could be co-opted and repurposed as phases in the developmental cycle of a propagule-forming lineage, thereby establishing novel reproductive programs. This agrees with previous experimental results where co-option was proposed as an explanation for the rapid evolution of unicellular propagules [17]. Our model explains how this process may take place, showing that pre-existing cell states coupling adhesion and cell behaviour could have been co-opted to regulate reproduction during the transition to multicellularity.

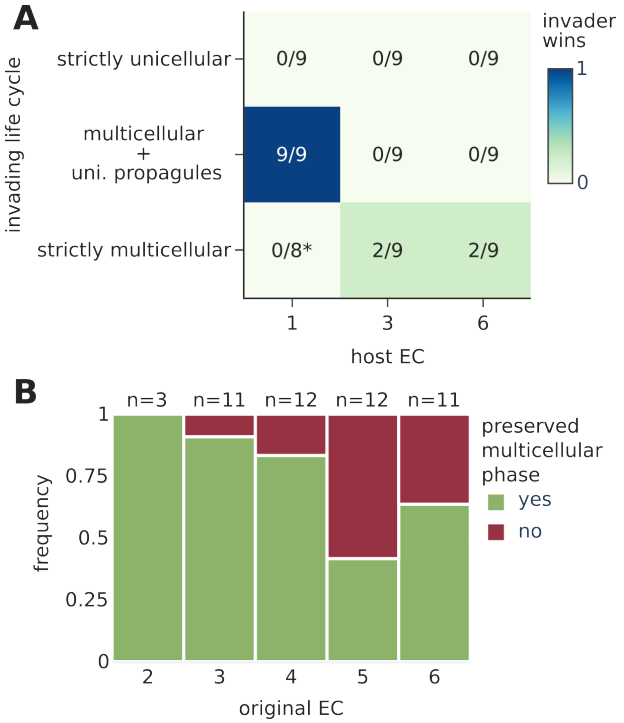

Figure 5. Multicellularity is evolutionarily protected in EC 1. **A** Number of competitions where the invading strategy wins against the host strategy. We compete three invading lineages with different life cycles against three host lineages in ECs 1, 3, and 6. Lineages were selected based on their putative fitness (see Methods, Measure of fitness) in the environment hosting the competition. The asterisk marks one data point that we excluded because neither lineage outcompeted the other in the simulation. Mutations were disabled in these simulations to prevent further evolution. **B** Frequency of initially multicellular strategies that preserved a multicellular phase after being transferred to EC 1 for 10^8 time steps.

The eco-evolutionary feedback between cells and sources of food in our model recapitulates real-life examples of ecology shaping the evolution of life cycles, and therefore provides a possible explanation for their evolution. Organisms that alternate between unicellular and multicellular lifestyles often rely on fluctuations of nutrient availability to regulate switches between these stages. Similarly to how propagule-forming lineages in our model migrate as a multicellular cluster during a feeding stage and then produce propagules after food is depleted, many amoebozoans and opisthokonts perform collective feeding when resources are abundant, followed by unicellular reproduction through single-celled structures once food becomes scarce [14]. For example, the holomycotan *Fonticula alba* forms cell collectives that feed on patches of bacteria and later differentiate into a sorocarp for reproduction through spores [27]. Collective feeding followed by unicellular reproduction has also been described in Myxogastria [51–53],

Labyrinthulomycota [54, 55], and choanoflagellates like *Salpingoeca rosetta* [56–58]. Other choanoflagellates, like *Choanoeca flexa*, instead use alternative environmental signals like salinity to regulate a transition to the multicellular stage [59]. Interestingly, this species in particular forms multicellular groups both through aggregation and continued cell division, similarly to the cells in our simulations.

Once multicellular lineages evolved in our simulations, they could successfully colonise environments with more homogeneous resources (EC 1), although multicellularity could not evolve there from scratch. This may be due to unicellular strategies being more adaptive than weakly adhering strategies in this environment. Once lineages become unicellular, we see that mutations that generate sufficiently adhering clusters also become rare. By allowing cells to first evolve multicellularity and propagules in the intermediate environment (EC 3) before invasion of EC 1, this ecological interference between unicellularity and weak multicellularity is avoided. This phenomenon is reminiscent of environmental scaffolding, where fitness valleys for the evolution of multicellularity are removed by a change in environment [60], and where the environment itself (here the heterogeneous food patches and chemoattractant gradients) may encourage cells to cluster [61–63].

To conclude, the defining feature of the evolutionary transition to multicellularity is the explosion of morphological diversity it enabled. These innovations arise through the co-option of a pre-existing genetic and trait toolkit, re-purposed to organize and regulate form and function in the new multicellular context. Our model captures this *constructive* form of evolutionary innovation [64].

Methods

Our model consists of an evolving population of cells living in a two-dimensional arena. Cells must consume resources to survive and replicate. Resources are patchily distributed and release a chemical signal that cells can follow through chemotaxis. Each cell contains a GRN represented as a Boolean network. The expression of different genes in the GRN determines whether the cell is migrating or dividing and whether it adheres to neighbouring cells.

Following the CPM formalism, we implement a Hamiltonian equation which describes the energy of the system. A Monte Carlo method is then used to minimise this energy by accepting or rejecting copy attempts between pairs of lattice sites. The source code of the model was built on top of the Tissue Simulation Toolkit framework [38] and can be found at https://github.com/aleferna12/regulation_evolution2. Parameters used for the simulations are available in Table S 1.

Cellular Potts Model

Cells are modeled in a square lattice $\Lambda_{\text{cell}} \subset \mathbb{Z}$ of size $L^2 = 2000 \times 2000$. A cell c is composed of lattice sites x that share the same spin s, i.e. $c(s) = \{x \mid x \in \Lambda_{\text{cell}} \wedge \sigma(x) = s\}$. The configuration of spins on the lattice is updated stochastically according to a Metropolis algorithm. Each MCS, we randomly sample L^2 sites x from the lattice and select a site $x' \in$ neigh(x) in their Moore neighbourhood, which may copy its spin $\sigma(x')$ into x. The probability that this copy attempt is successful depends on the difference that it would incur to the energy H of the system, described by a Hamiltonian function, as well as the migration biases $Y(x,x')$:

$$H = H_{\text{size}} + H_{\text{adh}}$$

$$Y(x,x') = Y_{\text{pers}}(x,x') + Y_{\text{chem}}(x,x')$$

If a copy attempt would result in a decrease in the total energy of the system, i.e. $\Delta H + Y(x,x') < 0$, it is always accepted. Otherwise, a Boltzmann distribution is used to calculate the probability that the copy attempt might still succeed due to random “thermal" fluctuations in the environment:

$$P\left(\Delta H, Y(x,x')\right) = e^{-\frac{\Delta H + Y(x,x')}{T}}$$

where $T = 16$ is the Boltzmann temperature. To increase computational efficiency, we restrict sampling to cell boundaries following the implementation of van Steijin et al. [65].

Cell size maintenance. The area of a cell $A(c) = |c|$ fluctuates around the target area parameter $A_{\text{t}} = 50$. Deviations from this target increase the system's total energy (represented by the term H_{size} in the Hamiltonian equation):

$$H_{\text{size}} = \sum_{c \in C} \lambda \times (A(c) - A_{\text{t}})^2$$

where C is the set of cells and $\lambda = 4$ is the resistence of cells to deviations in area.

Table 1. Model parameters

Parameter	Explanation	Value
L	size of the square lattice	2000 lattice sites
T	Boltzmann temperature	16 AUE
λ	cell stiffness	4 AUE/[lattice site]^2
A_t	target area of a cell	50 lattice sites
Cell adhesion		
J_α	minimum contact energy between cells	12 AUE
J'_α	contact energy between the cells and the medium	24 AUE
ν	number of ligands and receptors per cell	8 ligands–receptors
Cell migration		
μ_{pers}	strength of persistent migration	3 AUE
μ_{chem}	strength of chemotaxis	1 AUE
k_χ	scaling factor chemoattractant gradient	0.05 mol/[lattice site length]
Cell division		
η_{init}	delay before the start of division	400 MCS
η_{grow}	time for dividing cell to grow $2 \times A_{\text{t}}$ and divide	2×10^4 MCS
Food and metabolism		
τ_{eat}	refraction period of consumption of food	2 MCS
τ_{met}	metabolic period	100 MCS
Γ	maximum number of food units supported on Λ_{food}	524288
Evolution		
g	period between GRN updates	20 MCS
m	mutation probability	0.05
σ_{mut}	standard deviation of mutation size	0.05
ζ	death probability	5×10^{-6}

Cell adhesion. The total contact energy resulting from interactions between neighbouring cells is implemented as the H_{adh} term in the Hamiltonian:

$$H_{\text{adh}} = \sum_{(x,x')} J(\sigma(x), \sigma(x')) \times (1 - \delta(\sigma(x), \sigma(x')))$$

$$\delta(a,b) = \begin{cases} 1 & \text{if } a = b \\ 0 & \text{otherwise} \end{cases}$$

where (x, x') are all pairs of neighbouring sites on the lattice, such that $x' \in$ neigh(x). Calculations are restricted to cell boundaries by the Kronecker delta δ. The contact energy of a pair of sites with different spins $J(s_1, s_2)$ is proportional to the similarity of the vectors of expression states of ligand $I(s)$ and receptor $R(s)$ genes of the cells associated with the two spins:

$$J(s_1, s_2) = J_\alpha + \text{sim}(R(s_1), I(s_2)) + \text{sim}(R(s_2), I(s_1))$$

$$\text{sim}(R, I) = \sum_{i=1}^{\nu} i\delta(R_i, I_i)$$

where $J_\alpha = 12$ is the minimum contact energy between any two cells, and ν is the number of receptor and ligand genes of the cells. We assume that the medium is inert and that the contact energy between a cell and the medium is constant, such that in the special case where either s_1 or s_2 is the spin that represents the medium s_{med}, then $J(s, s_{\text{med}}) = J'_\alpha$, where J'_α is a parameter with value 24. Thus, the strength $\gamma(s_1, s_2)$ with which two cells with spin s_1

and s_2 adhere can be described in terms of the difference between the contact energy of cells and the medium and the contact energy between the two cells:

$$\gamma(s_1, s_2) = J'_\alpha - \frac{J(s_1, s_2)}{2}$$

For our simulations, we chose values J_α, J'_α, and ν such that the range of possible $\gamma(s_1, s_2)$ between two cells is $[-18, 18]$, with negative values indicating that the cells do not adhere, and positive that they do.

Food and metabolism

Food is modelled in a separate lattice Λ_{food} with the same dimensions as Λ_{cell}. Throughout the simulation, we introduce food in Λ_{food} every $1/\phi$ MCS as a "patch" with area A_{food} in the approximate shape of a circle (Fig. 1A). When created, a food patch is composed of 64 layers of food units, representing a multilayer bacterial biofilm. We vary ϕ and A_{food} in our simulations to represent different environmental conditions (see Table S1 and Fig. S1). To decide where a new food patch is created, we query random positions on the lattice until we find one that is no closer than d_{min} to any food patch currently in the environment:

$$d_{\text{min}} = \frac{L}{\sqrt{2|\mathcal{P}|}}$$

where L is the size of the lattice and $\mathcal{P}$ is the set of food patches currently in the environment. We then centre the new food patch at this position. This is done to ensure that food patches are never created too close to each other and that cells always need to migrate across the environment to reach them. We set a maximum number of food units Γ allowed in $\Lambda_{\text{food}} = 524288$, such that a food patch creation attempt is cancelled if it would result in exceeding this limit. This is done for computational reasons, as the algorithm that selects a semi-random position for the food patch described above has a high rejection ratio when the food patch density is very high.

Cells that share a site x on Λ_{cell} with a corresponding site containing food y on Λ_{food} can consume one food unit from y provided that they have not eaten in the last $\tau_{\text{eat}} = 2$ MCS. When consumed, the food unit is removed from the lattice and added to the cell's metabolic reserves. The gradient emanating from a food patch is removed when the cells eat its last food unit. Every $\tau_{\text{met}} = 100$ MCS, we decrease the metabolic reserves of all cells by one unit of food, representing a metabolism. Therefore, the ratio $\frac{\tau_{\text{met}}}{\tau_{\text{eat}}}$ determines the rate at which cells can accumulate metabolic reserves. Cells that run out of metabolic reserves are considered dead and are removed from the lattice. Additionally, all cells have a probability $\zeta = 5 \times 10^{-6}$ of dying each MCS regardless of how much food they have accumulated. This probability accounts for death caused by processes we do not model explicitly, such as oxidative stress and predation.

Gene regulation

Each cell in a simulation contains a GRN with a fixed topology composed of three layers of genes that control its behaviour (Fig. 1B). The first layer consists of two sensory genes that provide the cell with information about (i) the local concentration of the chemoattractant signal that emanates from the food sources and (ii) the amount of metabolic reserves the cell has left to spend. These sensory genes are connected to a middle layer of $2\nu + 2 = 18$ regulatory genes representing a network of transcription factors that control each other's expression as well as the expression of the functional genes. Lastly, an output layer contains the functional genes that determine cell behaviour. The first of these genes determines the cell state (whether the cell is currently migrating or dividing), followed by ν ligand genes and ν receptor genes that together determine how strongly the cell adheres to its neighbours.

The expression state of regulatory and output genes in the network is boolean (either 0 - not expressed or 1 - expressed). Regulatory genes receive input both from the sensory genes (i.e. the chemical gradient and metabolic reserves of the cell) and from all regulatory genes, including themselves. Functional genes receive input only from genes in the regulatory layer. Every $g = 20$ MCS, chosen so we even out microscopic fluctuations in the cell parameters, we synchronously update the expression state of each gene i in the network as follows:

$$r_i(t+1) = \sum_{j \in \mathcal{N}_i^-} w_{j \to i} S_j(t)$$

$$S_i(t+1) = \begin{cases} 1 & \text{if } r_i > \rho_i \\ 0 & \text{otherwise} \end{cases}$$

where $\mathcal{N}_i^-$ is the set of in-neighbours of i and $r_i(t+1)$ is the total input into gene i coming from genes j with state S_j

at time t, which respectively regulate i with weight $w_{j\to i}$. $S_i(t+1)$ is then the new state of gene i, determined by whether r_i is larger than ρ_i, the threshold of activation for this gene.

Division

A cell will start division if the state of the first functional gene of its GRN is 1 for twenty consecutive GRN updates (corresponding to $\eta_{\text{init}} = 400$ MCS), representing a period during which the cell prepares its cellular machinery before the beginning of division. Once division starts, the cell can no longer migrate or perform chemotaxis, simulating the conflicting use of the cytoskeleton for division and migration characteristic of some microorganisms [1, 43]. During division, we progressively increase the target area of the cell at a fixed rate for $\eta_{\text{grow}} = 2\times 10^4$ MCS to $2A_{\text{t}}$, causing the cell to grow approximately twice its original size. At the end of this period, we divide it along its minor axis to form two daughter cells. Division is halted if the cell expresses 0 in its cell state gene at any point during this process, which will reset its cell state to migrating. When the cell divides, each weight and activation threshold in the GRN of one of the daughter cells has a $m = 0.05$ probability of mutating. If a mutation event occurs, we then add a small random number sampled from a normal distribution with mean 0 and $\sigma_{\text{mut}} = 0.05$ to the mutated network parameter. The other daughter cell inherits its genome from the mother unaltered. The metabolic reserves accumulated by the mother cell are equally partitioned between the daughters.

Migration

When the state of the cell state gene is 0 (or if it has been 1 for less than η_{init} MCS), the cell is in migrating mode. We model persistent migration by biassing the movement of a cell with spin s towards its previous direction of motion $\psi(s)$:

$$Y_{\text{pers}}(x,x') = -\mu_{\text{pers}}\cos\big(\psi(\sigma(x')) - \theta(s,x)\big)$$

where $\theta(s,x)$ is the angle between the centre of mass of the cell with spin s and the target site of the copy attempt, and μ_{pers} is the maximum energy bias of persistent migration, which we set to 3 for migrating cells and to 0 for dividing cells, making the latter stationery. $\psi(s)$ is updated every 50 MCS with the actual direction of motion of the cell during this period, resulting in cells that move consistently in the same direction over short time scales and display Brownian motion over long scales [46].

Chemotaxis

Migrating cells can also perform chemotaxis by following a noisy chemical signal that emanates from the sources of food, forming a gradient that decays linearly. We do not model diffusion for computational efficiency, and instead assume that the gradient is static. We model this chemical signal in a separate lattice Λ_{chem} with the same dimensions as Λ_{cell}. The concentration of the chemical signal $\chi(x)$ at site x is determined by its distance to the closest food patch:

$$\chi(x) = 1 + k_\chi \times (D - d_{\text{food}}(x))$$

$$d_{\text{food}}(x) = \min(\{d(x,p) \mid p \in \mathcal{P}\})$$

where $k_\chi = 0.05$ is a scaling constant which determines the slope of the gradient, D is the diagonal of the lattice, and $d(x,p)$ is the Euclidean distance between x and the centre of the food patch p. To add noise to the chemical gradient, we truncate non-integer values of χ to their integer part $\lfloor\chi\rfloor$ with probability $\chi - \lfloor\chi\rfloor$. Otherwise, they are changed to the closest integer larger than χ. To implement chemotaxis, we find the signal's centre of mass by averaging χ across the cell lattice sites. The chemoattractant direction is then given by the angle $\omega(s)$ spanning from the centre of mass of a cell with spin s to the centre of mass of the signal perceived by that cell. Chemotaxis occurs because the success rate of lattice site copy attempts performed by a cell is larger if their direction aligns with $\omega(s)$:

$$Y_{\text{chem}}(x,x') = -\mu_{\text{chem}}\cos\big(\omega(\sigma(x')) - \theta(s,x)\big)$$

where μ_{chem} is the maximum energy bias of chemotaxis, which we set to 1 for migrating cells and to 0 for dividing cells. Note that the speed of a single cell's chemotaxis depends on the slope of the gradient (due to averaging X), which is constant across simulations.

Selective advantages of multicellularity and unicellularity

To confirm that collective migration enhances survival rates in heterogeneous environments, we transfer strictly unicellular lineages to EC 6. In this environmental condition, the inability of strictly unicellular lineages to form multicellular clusters results in slower migration and high death rates due to starvation (Video S5, Fig. S2A and B). Conversely, to investigate the effect of higher dispersal rates on homogeneous environments, we placed high-adhesion

multicellular lineages in EC 1, showing that they struggle to take advantage of the food available because the clusters cannot easily divide and spread through the environment, forcing all of the constituent cells to compete for the same resource-poor food patches (Video S6, Fig. S2C and D).

Non-evolutionary simulations

After obtaining the results from our evolutionary simulations (as described in Results, Model setup), we ran a set of non-evolutionary simulations where mutations are disabled. The purpose of these simulations was to build a large, fine-grained dataset that we can use to analyse functional traits of the life cycles that evolve in our model. We start each simulation with 100 cells cloned from an evolved lineage's most recent common ancestor (MCRA), which ensures that cell behaviour is consistent throughout the simulation and representative of the evolved population. Then, we run the simulation for 10^6 MCS while the population grows towards equilibrium and readjusts to its environment. After that, we run the simulation for another 10^6 MCS while we record the data used for the analyses described below. Data points are recorded every 20,000 MCS.

Categorisation of life cycles

We categorise the life cycles evolved in the simulations into three groups: strictly unicellular, multicellular + unicellular propagules, and strictly multicellular. We start by recording all unique combinations of adhesion proteins expressed by the cells in a non-evolutionary simulation (see Methods, Non-evolutionary simulations), storing them in the vector E. We also store the frequency with which each combination of adhesion genes was expressed by the cells according to their cell state in the vectors F^{mig} and F^{div}, such that F_i^{mig} is the frequency with which a cell in the simulation is both migrating and expressing E_i. We then calculate the median adhesion strength between cells, given their cell states:

$$\widetilde{\gamma}_{t_1,t_2} = \text{wmed}(A, W)$$

$$A = [\gamma(E_i, E_j) \mid 0 \leq i, j < |E|]$$

$$W = [F_i^{t_1} \times F_j^{t_2} \mid 0 \leq i, j < |E|]$$

where t_1 and t_2 are cell states (either migrating, dividing, or all, in which case $F^{\text{all}} = F^{\text{mig}} + F^{\text{div}}$), wmed$(A, W)$ gives the median of A weighted by the vector W, and $\gamma(E_i, E_j)$ is the adhesion strength calculated by comparing the vectors of expression of adhesion proteins E_i and E_j expressed by cells with sigmas s_i and s_j respectively, such that $\gamma(E_i, E_j) = \gamma(s_i, s_j)$ (see Methods, Cell adhesion).

This gives us six combinations of adhesion strength $\widetilde{\gamma}$ values between the different cell states: $\widetilde{\gamma}_{\text{mig,mig}}$, $\widetilde{\gamma}_{\text{mig,div}}$, $\widetilde{\gamma}_{\text{mig,all}}$, $\widetilde{\gamma}_{\text{div,div}}$, $\widetilde{\gamma}_{\text{div,all}}$, and $\widetilde{\gamma}_{\text{all,all}}$. We usually abbreviate $\widetilde{\gamma}_{t,\text{all}}$ to simply $\widetilde{\gamma}_t$, for example $\widetilde{\gamma}_{\text{div,all}} = \widetilde{\gamma}_{\text{div}}$ in the text and figures. To classify a life cycle, we then first ask whether migrating cells most frequently adhere to other migrating cells (i.e. $\widetilde{\gamma}_{\text{mig,mig}} > 0$). If they do not, we classify the life cycle as strictly unicellular. Otherwise, we then ask whether dividing cells most frequently adhere to other dividing cells (i.e. $\widetilde{\gamma}_{\text{div,div}} > 0$). If they do not, we classify the life cycle as multicellular + unicellular propagules. Otherwise, we classify the life cycle as strictly multicellular, and use $\widetilde{\gamma}_{\text{div}}$ to differentiate between lineages that often form propagules ($\widetilde{\gamma}_{\text{div}} \approx 0$, green in Fig. 2) and those that never or rarely do ($\widetilde{\gamma}_{\text{div}} \gg 0$, yellow in Fig. 2).

In Fig. 4, we examine the evolution of propagule formation across $1e8$ MCS. Because the evolutionary simulation contains only a few cells of the lineage of interest, we cannot directly extract enough data to run the analysis as described above. Instead, to calculate the γ values displayed in Fig. 4, we artificially feed the GRN of the lineage's ancestor with inputs experienced by other cells in the simulation, and then compare the GRN's outputs with data from the population in real-time during evolution. Sometimes, imprecisions associated with this method lead the algorithm to predict that all cells of an ancestor would migrate (or divide). In those cases, we cannot trivially assert the life cycle of the ancestor, and conservatively label it "undetermined" in the figure.

Measure of dispersal

To measure the dispersal of a lineage in its environment, we start by recording the positions of all cells in the lattice in a non-evolutionary simulation (see Methods, Non-evolutionary simulations). For each time step where we recorded cell positions, we then perform a standard quadrat analysis using a quadrat size of 100x100 lattice sites. We define the dispersal of the population at a time step t as:

$$d_t = 1 - \frac{\text{var}(Q_{\text{p}})}{\overline{Q}_{\text{p}}}$$

$$Q_{\text{p}} = \{q/N_t \mid q \in Q\}$$

where $\overline{Q}_{\mathsf{p}}$ is the mean of the set containing the proportion of cells in each quadrat Q_{p}, N_t is the population size at time t, and Q is a set containing the number of cells on each quadrat at time step t. This ensures that our dispersal metric d_t lies in the interval $(0, 1]$, where ≈ 0 represents the situation where all cells are contained in a single quadrat and 1 represents the situation where each quadrat contains the same number of cells. Finally, we define the dispersal of the lineage as the mean of all of its recorded d_t (measured every 20,000 MCS in non-evolutionary simulations, see Methods, Non-evolutionary simulations).

Measure of fitness

We consider the fitness of a population to be proportional to how much food it can consume from its environment before reaching equilibrium with the influx rate of food. Populations that can empty the environment of food before reaching equilibrium are considered to have fitness $f = 1$, while those that require the lattice to be full to survive have fitness $f = 0$. f is calculated by taking the mean of the time series of f_t, measured every 20,000 MCS in non-evolutionary simulations (see Methods, Non-evolutionary simulations) as $f_t = 1 - \beta_t/\Gamma$, where β_t is the number of food units on Λ_{food} at time step t and Γ is the maximum amount of food supported on the lattice.

References

[1] Richard K. Grosberg and Richard R. Strathmann. "The Evolution of Multicellularity: A Minor Major Transition?" en. In: *Annual Review of Ecology, Evolution, and Systematics* 38.Volume 38, 2007 (Dec. 2007), pp. 621–654. ISSN: 1543-592X, 1545-2069. DOI: 10.1146/annurev.ecolsys.36.102403.114735.

[2] Yuanxiao Gao, Arne Traulsen, and Yuriy Pichugin. "Interacting cells driving the evolution of multicellular life cycles". en. In: *PLOS Computational Biology* 15.5 (May 2019). Ed. by Natalia L. Komarova, e1006987. ISSN: 1553-7358. DOI: 10.1371/journal.pcbi.1006987.

[3] R. K. Grosberg and R. R. Strathmann. "One cell, two cell, red cell, blue cell: The persistence of a unicellular stage in multicellular life histories". In: *Trends in Ecology & Evolution* 13.3 (Mar. 1998), pp. 112–116. ISSN: 0169-5347. DOI: 10.1016/S0169-5347(97)01313-X.

[4] Yoshinori Kawabe et al. "Evolution of multicellularity in Dictyostelia". In: *The International journal of developmental biology* 63.8-9-10 (Jan. 2019), pp. 359–369. ISSN: 0214-6282. DOI: 10.1387/ijdb.190108ps.

[5] Anja Kamp, Hans Røy, and Heide N. Schulz-Vogt. "Video-supported Analysis of Beggiatoa Filament Growth, Breakage, and Movement". en. In: *Microbial Ecology* 56.3 (Oct. 2008), pp. 484–491. ISSN: 1432-184X. DOI: 10.1007/s00248-008-9367-x.

[6] František Adamec, David Kaftan, and Ladislav Nedbal. "Stress-Induced Filament Fragmentation of Calothrix Elenkinii (cyanobacteria) Is Facilitated by Death of High-Fluorescence Cells". en. In: *Journal of Phycology* 41.4 (2005), pp. 835–839. ISSN: 1529-8817. DOI: 10.1111/j.1529-8817.2005.00104.x.

[7] Ester Cecere, Antonella Petrocelli, and Marc Verlaque. "Vegetative reproduction by multicellular propagules in Rhodophyta: an overview". en. In: *Marine Ecology* 32.4 (2011), pp. 419–437. ISSN: 1439-0485. DOI: 10.1111/j.1439-0485.2011.00448.x.

[8] Jean-Luc Jany and Teresa E. Pawlowska. "Multinucleate Spores Contribute to Evolutionary Longevity of Asexual Glomeromycota." In: *The American Naturalist* 175.4 (Apr. 2010), pp. 424–435. ISSN: 0003-0147. DOI: 10.1086/650725.

[9] Helena M. P. Garcês et al. "Evolution of asexual reproduction in leaves of the genus Kalanchoë". In: *Proceedings of the National Academy of Sciences* 104.39 (Sept. 2007), pp. 15578–15583. DOI: 10.1073/pnas.0704105104.

[10] Li-Min Zhang et al. "Growth and Morphological Responses of Duckweed to Clonal Fragmentation, Nutrient Availability, and Population Density". English. In: *Frontiers in Plant Science* 11 (May 2020). ISSN: 1664-462X. DOI: 10.3389/fpls.2020.00618.

[11] Matthew Clements et al. "Forever fissiparous: asexual propagation and stable demography in a tropical and geographically isolated asterinid sea star". en. In: *Marine Biology* 166.6 (May 2019), p. 69. ISSN: 1432-1793. DOI: 10.1007/s00227-019-3518-0.

[12] Bernd Schierwater et al. "The enigmatic Placozoa part 1: Exploring evolutionary controversies and poor ecological knowledge". en. In: *BioEssays* 43.10 (2021), p. 2100080. ISSN: 1521-1878. DOI: 10.1002/bies.202100080.

[13] Ilya A. Gavrilov-Zimin. "Ancient reproductive modes and criteria of multicellularity". en. In: *Comparative Cytogenetics* 17 (Oct. 2023), pp. 195–238. ISSN: 1993-078X, 1993-0771. DOI: 10.3897/compcytogen.17.109671.

[14] Łukasz Lamża. "Diversity of 'simple' multicellular eukaryotes: 45 independent cases and six types of multicellularity". en. In: *Biological Reviews* 98.6 (Dec. 2023), pp. 2188–2209. ISSN: 1464-7931, 1469-185X. DOI: 10.1111/brv.13001.

[15] Martin E. Boraas, Dianne B. Seale, and Joseph E. Boxhorn. "Phagotrophy by a flagellate selects for colonial prey: A possible origin of multicellularity". en. In: *Evolutionary Ecology* 12.2 (Feb. 1998), pp. 153–164. ISSN: 0269-7653, 1573-8477. DOI: 10.1023/A:1006527528063.

[16] William C. Ratcliff et al. "Experimental evolution of multicellularity". en. In: *Proceedings of the National Academy of Sciences* 109.5 (Jan. 2012), pp. 1595–1600. ISSN: 0027-8424, 1091-6490. DOI: 10.1073/pnas.1115323109.

[17] William C. Ratcliff et al. "Experimental evolution of an alternating uni- and multicellular life cycle in Chlamydomonas reinhardtii". en. In: *Nature Communications* 4.1 (Nov. 2013), p. 2742. ISSN: 2041-1723. DOI: 10.1038/ncomms3742.

[18] Matthew D. Herron et al. "De novo origins of multicellularity in response to predation". en. In: *Scientific Reports* 9.1 (Feb. 2019), p. 2328. ISSN: 2045-2322. DOI: 10.1038/s41598-019-39558-8.

[19] Denis Roze and Richard E. Michod. "Mutation, Multilevel Selection, and the Evolution of Propagule Size during the Origin of Multicellularity." In: *The American Naturalist* 158.6 (Dec. 2001), pp. 638–654. ISSN: 0003-0147. DOI: 10.1086/323590.

[20] István Oszoli and István Zachar. "Group-selection via aggregative propagule-formation enables cooperative multicellularity in an individual based, spatial model". en. In: *PLOS Computational Biology* 20.5 (May 2024). Ed. by Yuriy Pichugin, e1012107. ISSN: 1553-7358. DOI: 10.1371/journal.pcbi.1012107.

[21] Eric Libby et al. "Geometry Shapes Evolution of Early Multicellularity". en. In: *PLOS Computational Biology* 10.9 (Sept. 2014), e1003803. ISSN: 1553-7358. DOI: 10.1371/journal.pcbi.1003803.

[22] Yuriy Pichugin et al. "Fragmentation modes and the evolution of life cycles". en. In: *PLOS Computational Biology* 13.11 (Nov. 2017), e1005860. ISSN: 1553-7358. DOI: 10.1371/journal.pcbi.1005860.

[23] Yuanxiao Gao et al. "Evolution of reproductive strategies in incipient multicellularity". In: *Journal of The Royal Society Interface* 19.188 (Mar. 2022), p. 20210716. DOI: 10.1098/rsif.2021.0716.

[24] Merlijn Staps, Jordi van Gestel, and Corina E. Tarnita. "Emergence of diverse life cycles and life histories at the origin of multicellularity". In: *Nature Ecology & Evolution 2019 3:8* 3.8 (July 2019), pp. 1197–1205. ISSN: 2397-334X. DOI: 10.1038/s41559-019-0940-0.

[25] Yuriy Pichugin, Hye Jin Park, and Arne Traulsen. "Evolution of simple multicellular life cycles in dynamic environments". In: *Journal of The Royal Society Interface* 16.154 (May 2019), p. 20190054. DOI: 10.1098/rsif.2019.0054.

[26] Jordi van Gestel and Martin A. Nowak. "Phenotypic Heterogeneity and the Evolution of Bacterial Life Cycles". en. In: *PLOS Computational Biology* 12.2 (Feb. 2016), e1004764. ISSN: 1553-7358. DOI: 10.1371/journal.pcbi.1004764.

[27] Christopher Toret et al. "The cellular slime mold Fonticula alba forms a dynamic, multicellular collective while feeding on bacteria". English. In: *Current Biology* 32.9 (May 2022), 1961–1973.e4. ISSN: 0960-9822. DOI: 10.1016/j.cub.2022.03.018.

[28] John H Koschwanez, Kevin R Foster, and Andrew W Murray. "Improved use of a public good selects for the evolution of undifferentiated multicellularity". In: *eLife* 2 (Apr. 2013). Ed. by Diethard Tautz, e00367. ISSN: 2050-084X. DOI: 10.7554/eLife.00367.

[29] Kai Tong, G Ozan Bozdag, and William C Ratcliff. "Selective drivers of simple multicellularity". In: *Current Opinion in Microbiology* 67 (June 2022), p. 102141. ISSN: 1369-5274. DOI: 10.1016/j.mib.2022.102141.

[30] Thibaut Brunet and Nicole King. "The Origin of Animal Multicellularity and Cell Differentiation". en. In: *Developmental Cell* 43.2 (Oct. 2017), pp. 124–140. ISSN: 15345807. DOI: 10.1016/j.devcel.2017.09.016.

[31] Arnau Sebé-Pedrós, Bernard M. Degnan, and Iñaki Ruiz-Trillo. "The origin of Metazoa: a unicellular perspective". en. In: *Nature Reviews Genetics* 18.8 (Aug. 2017), pp. 498–512. ISSN: 1471-0056, 1471-0064. DOI: 10.1038/nrg.2017.21.

[32] Monika Abedin and Nicole King. "Diverse evolutionary paths to cell adhesion". In: *Trends in cell biology* 20.12 (Dec. 2010), pp. 734–742. ISSN: 0962-8924. DOI: 10.1016/j.tcb.2010.08.002.

[33] Paul S. Murray and Ronen Zaidel-Bar. "Pre-metazoan origins and evolution of the cadherin adhesome". In: *Biology Open* 3.12 (Nov. 2014), pp. 1183–1195. ISSN: 2046-6390. DOI: 10.1242/bio.20149761.

[34] Erik R. Hanschen et al. "The Gonium pectorale genome demonstrates co-option of cell cycle regulation during the evolution of multicellularity". en. In: *Nature Communications* 7.1 (Apr. 2016), p. 11370. ISSN: 2041-1723. DOI: 10.1038/ncomms11370.

[35] Alan C. Love and Günter P. Wagner. "Co-option of stress mechanisms in the origin of evolutionary novelties". en. In: *Evolution* 76.3 (2022), pp. 394–413. ISSN: 1558-5646. DOI: 10.1111/evo.14421.

[36] Jordi van Gestel and Corina E. Tarnita. "On the origin of biological construction, with a focus on multicellularity". In: *Proceedings of the National Academy of Sciences* 114.42 (Oct. 2017), pp. 11018–11026. DOI: 10.1073/pnas.1704631114.

[37] Pierrick Bourrat et al. "Individuality Through Ecology: Rethinking the Evolution of Complex Life From an Externalist Perspective". en. In: *Ecology and Evolution* 14.12 (2024), e70661. ISSN: 2045-7758. DOI: 10.1002/ece3.70661.

[38] Josephine T. Daub and Roeland M.H. Merks. "Cell-based computational modeling of vascular morphogenesis using Tissue Simulation Toolkit". In: *Methods in Molecular Biology* 1214 (2015), pp. 67–127. ISSN: 10643745. DOI: 10.1007/978-1-4939-1462-3_6.

[39] James G. Umen. "Volvox and volvocine green algae". In: *EvoDevo* 11.1 (July 2020), p. 13. ISSN: 2041-9139. DOI: 10.1186/s13227-020-00158-7.

[40] Núria Ros-Rocher et al. "The origin of animals: an ancestral reconstruction of the unicellular-to-multicellular transition". In: *Open Biology* 11.2 (Feb. 2021). ISSN: 20462441. DOI: 10.1098/RSOB.200359.

[41] Qingyou Du et al. "The Evolution of Aggregative Multicellularity and Cell–Cell Communication in the Dictyostelia". en. In: *Journal of Molecular Biology* 427.23 (Nov. 2015), pp. 3722–3733. ISSN: 00222836. DOI: 10.1016/j.jmb.2015.08.008.

[42] Sanea Sheikh et al. "The Acrasis kona genome and developmental transcriptomes reveal deep origins of eukaryotic multicellular pathways". en. In: *Nature Communications* 15.1 (Nov. 2024), p. 10197. ISSN: 2041-1723. DOI: 10.1038/s41467-024-54029-z.

[43] David L. Kirk. *Volvox: A Search for the Molecular and Genetic Origins of Multicellularity and Cellular Differentiation*. en. Cambridge University Press, 1998. ISBN: 978-0-521-45207-6.

[44] Nicole King. "The Unicellular Ancestry of Animal Development". en. In: *Developmental Cell* 7.3 (Sept. 2004), pp. 313–325. ISSN: 15345807. DOI: 10.1016/j.devcel.2004.08.010.

[45] Marine Olivetta et al. "A multicellular developmental program in a close animal relative". en. In: *Nature* (Nov. 2024), pp. 1–8. ISSN: 1476-4687. DOI: 10.1038/s41586-024-08115-3.

[46] Joost B. Beltman et al. "Lymph node topology dictates T cell migration behavior". In: *Journal of Experimental Medicine* 204.4 (Mar. 2007), pp. 771–780. ISSN: 0022-1007. DOI: 10.1084/jem.20061278.

[47] Enrico Sandro Colizzi, Renske M.A. Vroomans, and Roeland M.H. Merks. "Evolution of multicellularity by collective integration of spatial information". In: *eLife* 9 (Oct. 2020), pp. 1–57. ISSN: 2050084X. DOI: 10.7554/ELIFE.56349.

[48] François Graner and James A. Glazier. "Simulation of biological cell sorting using a two-dimensional extended Potts model". In: *Physical Review Letters* 69.13 (Sept. 1992), pp. 2013–2016. DOI: 10.1103/PhysRevLett.69.2013.

[49] Nicole King et al. "The genome of the choanoflagellate Monosiga brevicollis and the origin of metazoans". en. In: *Nature* 451.7180 (Feb. 2008), pp. 783–788. ISSN: 0028-0836, 1476-4687. DOI: 10.1038/nature06617.

[50] Renske M. A. Vroomans and Enrico Sandro Colizzi. "Evolution of selfish multicellularity: collective organisation of individual spatio-temporal regulatory strategies". en. In: *BMC Ecology and Evolution* 23.1 (July 2023), p. 35. ISSN: 2730-7182. DOI: 10.1186/s12862-023-02133-x.

[51] Steven L. Stephenson. "Past and Ongoing Field-Based Studies of Myxomycetes". In: *Microorganisms* 11.9 (Sept. 2023), p. 2283. ISSN: 2076-2607. DOI: 10.3390/microorganisms11092283.

[52] Sydney E Everhart and Harold W Keller. "Life history strategies of corticolous myxomycetes: the life cycle, plasmodial types, fruiting bodies, and taxonomic orders". In: *Fungal Diversity* 29.1 (2008), pp. 1–16.

[53] Pauline Schaap et al. “The Physarum polycephalum Genome Reveals Extensive Use of Prokaryotic Two-Component and Metazoan-Type Tyrosine Kinase Signaling”. In: *Genome Biology and Evolution* 8.1 (Jan. 2016), pp. 109–125. ISSN: 1759-6653. DOI: 10.1093/gbe/evv237.

[54] “Labyrinthulomycota”. en. In: *Handbook of the Protists*. Ed. by John M. Archibald, Alastair G.B. Simpson, and Claudio H. Slamovits. Cham: Springer International Publishing, 2017, pp. 507–542. ISBN: 978-3-319-28147-6 978-3-319-28149-0. DOI: 10.1007/978-3-319-28149-0.

[55] Izumi Iwata et al. “Bothrosome Formation in *Schizochytrium aggregatum* (Labyrinthulomycetes, Stramenopiles) during Zoospore Settlement”. In: *Protist* 168.2 (Apr. 2017), pp. 206–219. ISSN: 1434-4610. DOI: 10.1016/j.protis.2016.12.002.

[56] Stephen R Fairclough et al. “Premetazoan genome evolution and the regulation of cell differentiation in the choanoflagellate Salpingoeca rosetta”. en. In: *Genome Biology* 14.2 (2013), R15. ISSN: 1465-6906. DOI: 10.1186/gb-2013-14-2-r15.

[57] Rosanna A. Alegado et al. “A bacterial sulfonolipid triggers multicellular development in the closest living relatives of animals”. eng. In: *eLife* 1 (Oct. 2012), e00013. ISSN: 2050-084X. DOI: 10.7554/eLife.00013.

[58] Stephen R. Fairclough, Mark J. Dayel, and Nicole King. “Multicellular development in a choanoflagellate”. en. In: *Current Biology* 20.20 (Oct. 2010), R875–R876. ISSN: 09609822. DOI: 10.1016/j.cub.2010.09.014.

[59] Núria Ros-Rocher et al. *Clonal-aggregative multicellularity entrained by salinity in one of the closest relatives of animals*. en. Oct. 2024. DOI: 10.1101/2024.03.25.586565.

[60] Guilhem Doulcier et al. “Stability of ecologically scaffolded traits during evolutionary transitions in individuality”. en. In: *Nature Communications* 15.1 (Aug. 2024), p. 6566. ISSN: 2041-1723. DOI: 10.1038/s41467-024-50625-1.

[61] Andrew J. Black, Pierrick Bourrat, and Paul B. Rainey. “Ecological scaffolding and the evolution of individuality”. en. In: *Nature Ecology & Evolution* 4.3 (Mar. 2020), pp. 426–436. ISSN: 2397-334X. DOI: 10.1038/s41559-019-1086-9.

[62] Caroline J. Rose et al. “Meta-population structure and the evolutionary transition to multicellularity”. en. In: *Ecology Letters* 23.9 (2020), pp. 1380–1390. ISSN: 1461-0248. DOI: 10.1111/ele.13570.

[63] Adriano Bonforti and Ricard Solé. “Unicellular–multicellular evolutionary branching driven by resource limitations”. en. In: ().

[64] Enrico Sandro Colizzi, Paulien Hogeweg, and Renske M.A. Vroomans. “Modelling the evolution of novelty: a review”. en. In: *Essays in Biochemistry* 66.6 (Dec. 2022). Ed. by Alistair McGregor, Alexandra Buffry, and Renske Vroomans, pp. 727–735. ISSN: 0071-1365, 1744-1358. DOI: 10.1042/ebc20220069.

[65] Leonie van Steijn et al. “Computational modelling of cell motility modes emerging from cell-matrix adhesion dynamics”. en. In: *PLOS Computational Biology* 18.2 (Feb. 2022), e1009156. ISSN: 1553-7358. DOI: 10.1371/journal.pcbi.1009156.